The International Journal of Advanced Manufacturing Technology (2018) 95:4091–4100
https://doi.org/10.1007/s00170-017-1504-6

ORIGINAL ARTICLE

CFD research on particle movement and nozzle wear in the abrasive water jet cutting head

Zhengrong Qiang[1] · Meiping Wu[1] · Xiaojin Miao[1] · Rupy Sawhney[2]

Received: 13 June 2017 / Accepted: 17 December 2017 / Published online: 4 January 2018

Abstract
Particle velocity and movement in the high-pressure abrasive water jet (AWJ) heading are significant jet properties which deserve a better understanding for improving AWJ machining performance. In this paper, particle acceleration and movement trajectory in the jet field within AWJ cutting head were conducted based on the Euler-Lagrange approach and the discrete particle model (DPM) from a computational fluid dynamics (CFD) simulation study. The particle inlet position, particle inlet angle, and converge angle of focus tube were taken into consideration in the physical model. The models were then assessed qualitatively and quantitatively by previous experiment data. The results indicated that a particle inlet located at a high position could increase particles' exiting velocity and decrease nozzle wear. A steeper abrasive feed angle would improve the particle acceleration process and reduce radial velocity, resulting in less nozzle weight loss. The effects of converging part angle were analyzed as well. The obtained results would improve the machine efficiency of the workpiece, extend nozzle lifetime, and guide the future design of AWJ nozzle.

Keywords High-pressure abrasive water jet (AWJ) · Computational fluid dynamics (CFD) · Particle velocity and movement · Nozzle wear

1 Introduction

1.1 AWJ introduction

High-pressure abrasive water jet (AWJ) cutting is based on a technique developed by Elmo Smith and Leslie Tirrell in the 1930s in the field of liquid ablative blasting. It has been widely applied in industrial process for both ductile and brittle materials [1]. The AWJ machining owns a distinct advantage over other manufacturing tools, such as laser cutting, because there is barely thermal zone affecting the workpiece's internal structure [2]. The internal flow existing in this technology involves a three-phase flow mixture of water (liquid), air (gas), and abrasive garnets (solid) [3]. A typical AWJ system is driven by a high-speed water jet formed by a pump generating several hundred MPa pressure through a small water orifice of about 0.2–0.4 mm in diameter. Then, high-speed water jet reaches the mixing chamber generating negative pressure (compared with atmosphere pressure) which has a suction effect of abrasive particles (e.g., silica or garnet) and air. The air-abrasive feed pipe controls the particle quantity. Then all of three phases enter into the mixing chamber, and they will go into a focusing tube with a conically shaped inlet where it is used to align this mixture progress. The abrasive particles are accelerated and concentrated by energy exchange with the surrounding water jet in the focus tube. Figure 1a shows a commercial AWJ system in our center and a scheme of a typical AWJ cutting head [4–6].

1.2 Experimental analysis of AWJ system

As a crucial component of AWJ system, it is necessary to enhance cutting head design to improve machining performance, reducing energy consumption and boost use time. The classic design to input the water jet is the central entry on top of the cutting head. Abrasives and air enter the mixing chamber by Venturi effect, usually through a single-sided

✉ Zhengrong Qiang
qiangzhengrong001@hotmail.com

[1] School of Mechanical Engineering, Jiangnan University, Wuxi 214122, China

[2] School of Industrial and Systems Engineering, University of Tennessee, Knoxville, TN 37996-2315, USA

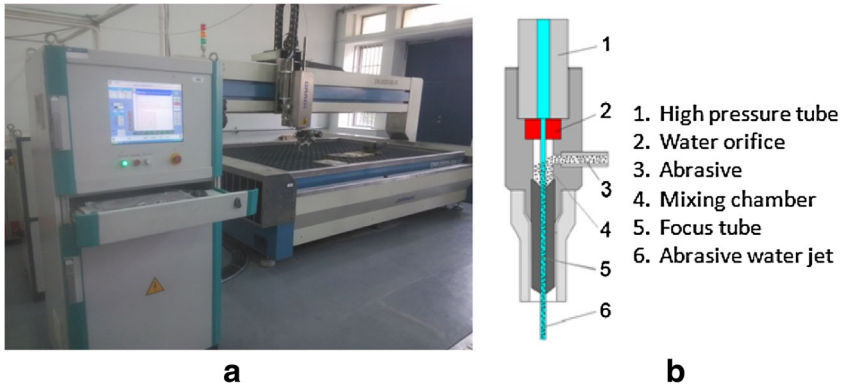

Fig. 1 **a** Practical AWJ system. **b** Schematic AWJ nozzle

input port. Most of cutting heads for injection-abrasive water jets are based on this solution [7]. However, even small geometrical variances have an impact on the cutting performance. It becomes clear that the study of the nozzle parameters along with a deeper understanding of the characteristics of multiphase flow inside nozzle head is essential through theoretical, experimental investigations and based on computational fluid dynamics (CFD) simulation [8].

Li et al. [9] investigated the influence based on the distance between the water jet orifice exit and focus tube entrance (converging part) on the cutting capability by using cut depth of the generated geometry as an optimization criterion. The researcher found that there exists an optimum distance with a corresponding maximum depth of cut. The cutting capability of the abrasive water jet improves up to 80% by selecting the proper distance between the orifice and focus. Osman [10] shows the influence of the mixing chamber length on the mass removal rate in two different materials. The mass removal rate decreases with an increase in the mixing chamber length up to a suitable value. The phenomenon is because with the extension of mixing chamber part of high-speed water rebound to the upper space concerning expansion effect.

1.3 Simulation analysis of AWJ system

Applying conventional measurements can get some optimum results. However, it cannot easily obtain a detailed information on inner cutting head. Meanwhile, it will also cost money and time to get corresponding optimum design parameter. To study such physical phenomenon and make it more economical, the CFD has become increasingly significant to obtain relative knowledge.

Chidambaram et al. [11] proposed a phenomenological model of the three-phase flow inside an AWJ machining cutting head with several improvements like taking into account the particle dimension distribution and effect of breakup of particles on the energy flux. The abrasive particle mean velocity at the exit plane of the focusing tube has been consistently validated through design of experiments. Huang [12] used CFD technology to simulate the velocity field of solid-liquid flow inside and outside the AWJ nozzle. The results indicate that there is a sudden growth in the jet velocity near the corner inside the nozzle, and then it remains steady in the focus tube. Teymoori [13] undertook a coupled Eulerian-Lagrangian approach to simulate the whole deformation process of a water jet incremental sheet metal forming of a conical part by 3D finite element method (FEM). Rongguo [14] investigate ultra-high pressure water jet (WJ) flow field with the high-frequency velocity vibration at the nozzle inlet through CFD method, which shows the clues of vibration and water jet parameters impacting the flow. Wang et al. [15] utilize a discrete element method-computational fluid dynamics (DEM–CFD) analysis to better investigate the dynamic characteristics of high-speed abrasive air jet (AAJ). Solid particles of micron sizes within the air jet are examined to determine the jet evolution and expansion as well as the particle distribution within the flow. Particularly, particle sphericity (shape factor from 0.65 to 0.9 [16]) is considered for the particle-fluid interaction in addition to the particle-particle collision.

1.4 The goal of this study

The goal of this study is the development and validation of an internal three-phase flow model of the abrasive water jet with the capability to predict the acceleration of solid particles and the wear of nozzle wall. As these two criterions are significant to AWJ outlet performance, 3D Euler-Lagrange numerical simulation is carried under different cutting head parameters such as particle inlet angle, inlet position, and converge part angle of focus tube. The study distinguishes itself from previous attempts by analyzing several hitherto unaddressed issues:

- It combines ANSYS Fluent package with Solidworks software, which makes it easy for designers to change the corresponding geometrical parameter.
- It presents a complete modeling progress for CFD simulation, making it easy for other scholars to conduct a similar study.
- It attempts a comprehensive validation of the simulated model using several previous experiment sets [17–20],

indicating the model has a good agreement with experimental data from three tested aspects.
- It analyzes three different nozzle structure factors and shows that they cannot be ignored considering their influence on maximum abrasive-particle acceleration and wear of the AWJ system, especially of the focus tube.

2 Numerical model

From the second picture of Fig. 1b, three phases (air, water, and particles) make up the abrasive water jet in the AWJ nozzle. Considering the practical application, the volume fraction of solid particles is generally between 8 and 12%, which means the Euler-Lagrange method is acceptable [21].

2.1 Fluid phase governing equations

Ultrahigh pressure WJ is a typical high turbulence flow. In order to simulate the two continuous phases, the multiphase Euler-Euler approach with water and air was employed, corresponding to the operation adopted in previous literature [22]. Compared with all the other multiphase models, this is the most complicated and accounts for a large number of computational resources. However, the multiphase Euler-Euler approach seems the most feasible to simulate a two-phase flow as it can model any volume of phases in any combination. Also, there is no any problem with phases exhibiting significant velocity differences in the nozzle [23].

In the Euler-Euler model, one constant pressure value is shared by all phases, while momentum and continuity equations are solved separately [24]. The description of multiphase flow as interpenetrating continua incorporates the concept of phase volume fractions, denoted here by α_p. The volume of phase p, V_p, is defined by

$$V_p = \int_V \alpha_p dV \tag{1}$$

where

$$\sum_{p=1}^{n} a_p = 1 \tag{2}$$

The continuity equation for the phase p is

$$\frac{\partial}{\partial t}\left(\alpha_p \rho_p\right) + \nabla\cdot\left(\alpha_p \rho_p \vec{v}_p\right) = \sum_{q=1}^{n}\left(\dot{m}_{qp} - \dot{m}_{pq}\right) + S_p \tag{3}$$

where $\vec{v}_p$ is the velocity of phase p, $\dot{m}_{qp}$ characterizes the mass transfer from the q^{th} to p^{th} phase and $\dot{m}_{pq}$ means an opposite situation.

The source term S_p in Eq. (3) is zero, but, if necessary, it is possible to specify a constant or user-defined mass source for each phase. A similar term appears in the momentum and enthalpy equations.

The jet velocity (v_{jet}) at the water orifice exit can be calculated through the Bernoulli equation adjusted by using a compressibility coefficient ψ as

$$v_{\text{jet}} = \psi\sqrt{2\frac{P - p_2}{\rho_2}} \tag{4}$$

where P is pump pressure given in MPa, ρ_2 is the density of water (kg/m^3) under the atmosphere condition, and p_2 is the mixing chamber pressure, and the compressibility coefficient is given as [25]

$$\psi = \sqrt{\frac{L}{P(1-n)}\left[\left(1 + \frac{P}{L}\right)^{(1-n)} - 1\right]} \tag{5}$$

where the model constants $L = 300$ MPa, and $n = 0.1368$ at 25 °C.

The mass flow rate of air ($\dot{m}_a$) as well as air velocity (v_a) can be obtained using the mixing chamber pressure. The length of the air delivery tube and its diameter are needed for the entrainment model. The mixing chamber pressure p_2, the mass flow rate of air, and air velocity can be calculated because of the pressure drop (Δp_m) by assuming fully developed pipe flow in the air delivery tube. The pressure drop over a pipe of length L_a with diameter D_a is given as

$$\Delta p_m = f_a\left(\frac{1}{2}\rho_a v_a^2\right)\frac{L_a}{D_2} \tag{6}$$

$$\dot{m}_a = Q\rho_a = v_a\frac{D_a^2}{4}\rho_a \tag{7}$$

where f_a is the friction factor and v_a is the bulk velocity of air in the tube.

2.2 Solid phase governing equations

It is a fact that abrasive particles are entrained with air by negative pressure in the mixing chamber resulting from the high-speed jet stream. As the solid phase volume percentage is low (less than 10–15%), one-way coupling strategy will be adopted in the case, which means that particle movement is affected by the water phase while the solid phase has no impact on the fluid flow. This assumption can be supported by previous literatures [5, 7, 8, 12]. In addition, 0.7–0.8 sphericity of particles are employed as it meets practical application and it can be set in corresponding software. Thus, particle trajectories

were computed based on the discrete particle model (DPM) [22]. An expression for the drag force, F_D, is modeled as

$$F_D = C_D \frac{\pi\rho}{8} d^2 w^2 + \frac{\pi\rho}{8} d^3 \dot{w} \tag{8}$$

where C_D is drag coefficient, d is the mean diameter of the spherical particle, w is a relative velocity between the abrasive particle and fluid, and the dot indicates time derivative. The first term on the right-hand side is due to viscous drag between the sphere and fluid under steady flow motion, while the second term is the inertia component due to relative acceleration.

The velocity of the abrasive particles v_p depends on the water jet velocity at the orifice outlet v_j, both measured in meters per second. The water mass flow rate $\dot{m}_w$ and the abrasive solid mass flow rate $\dot{m}_p$ are both measured in kilograms per second. The velocity of the particles can be determined by momentum conservation [25] as expressed in Eq. (9):

$$v_p = \eta \frac{v_j}{1 + \dot{m}_w / \dot{m}_p} \tag{9}$$

where η is the transfer efficiency of dimensionless momentum. The momentum transfer efficiency η was introduced by Hoogstrate [4] as Eq. (10):

$$\eta = c_1 - c_2 R \tag{10}$$

where c_1 and c_2 are constants obtained by experiment with typical values of 1 and 1.6, respectively, for a 1-mm nozzle diameter using #80 Barton garnet abrasive particles. In this section, R is the abrasive load ratio between the solid mass flow rate and the fluid mass flow rate.

2.3 Abrasive particle interaction during mixing and acceleration

These authors [17, 25] measure that about 70 to 80% of all particles are subjected to fragmentation and find that this number depends on the initial abrasive grain size pump pressure and focus diameter. They also show that changes in the focus length do not affect the particle size distribution, but changes in the mixing chamber design do influence the fragmentation behavior. The fragmentation of the abrasive particles absorbs a certain amount of the abrasive particles' kinetic energy. Bond's comminution formula [18] can be used to calculate the energy involved in this fragmentation process. The absorbed energy is

$$E_F = w_i \cdot \frac{\sqrt{d_{\mathrm{Pin}}} - \sqrt{d_{Pout}}}{\sqrt{d_{Pout}}} \cdot \sqrt{\frac{100}{d_{\mathrm{Pin}}}} \tag{11}$$

In Eq. (11), w_i is the index of workability that is estimated by comminution study, and d_{Pin} and d_{Pout} are particle inlet and out diameter, respectively.

3 Physical model and boundary conditions

3.1 Physical model

The mathematical models described above can be used to solve the multiphase flow problem involved in a typical abrasive water jet. Figure 2a shows the physical model of a conventional nozzle and the computational flow region: a quasi-3D internal flow field. 3D simulation is chosen for this experiment as it is more reliable compared with 2D simulation. The model was first modified in Solidworks software because it is user-friendly and easy to change corresponding parameters which saved time. According to the practical application and commercial principle, a simplified geometry of the cutting head was modeled. The system's nozzle geometry used in this study can be found in Table 1 [10, 18, 20], which are all based on current practical design. Then, the origin point (0, 0, 0) of the coordinate system is set at the center of the upper plane of converging part, meaning the end of mixing chamber and the beginning of focus tube. In this case, L is set as the length from orifice outlet to focusing tube exit in the direction of $-Z$, seen in Fig. 2a. The structured grids imported into the CFD simulations will be treated by different meshing strategies. In Fig. 2b, the mesh solution for the cutting head is reported (dimensions are in mm). For example, in the vertical axis direction where exists higher velocity and more intensive interaction than other places, the mesh grids will be finer by inflation process, while a coarse method is enough for outer surface. There are 789,780 nodes for the total mesh number in the current simulation based on aforementioned meshing strategy.

3.2 Boundary conditions and operating parameters

A CFD solver FLUENT was utilized to analyze the multi-fluid granular model describing the jet behavior of gas-fluid-solid mixture. Double precision was checked to get full node information at different dimension direction taking into consideration the extremely high speed and short time frame mixing progress, resulting in longer time but more accurate results. The parallel option was checked by entering four numbers of CPUs to decrease computing time. Mesh check was the first step to make sure that there is no adverse volume value or incompatible grid before setting operating parameter. The gravity setting was − 9.81 m/s in Z-positive axis direction.

Assuming that the fluid is incompressible and viscous, the Re is much higher than 3000, which is the criterion for the inception of flow turbulence. Therefore, in Fluent, the

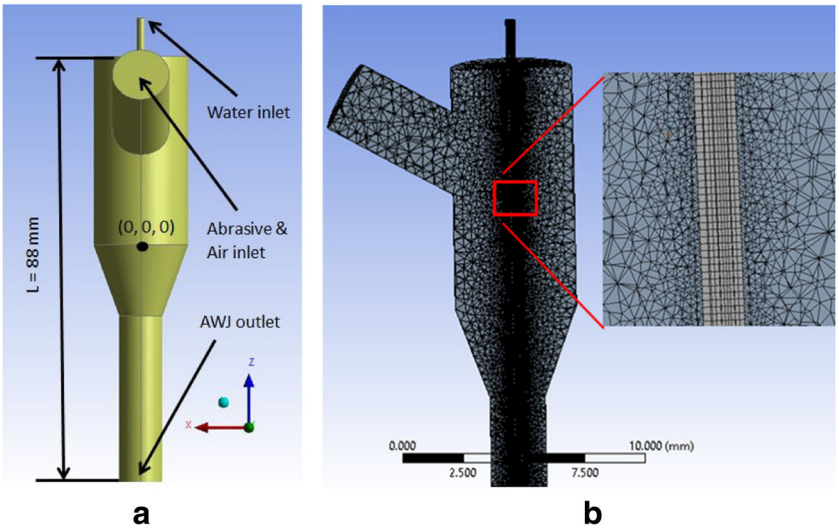

Fig. 2 Model of the cutting head (**a**) and mesh solution (**b**)

realizable $k-\varepsilon$ turbulence equations are used as the governing equations due to its advantages of accurate prediction of plane and circle jet [23], and the transport equations for the turbulence energy k and dissipation rate ε are

$$\frac{\partial(\rho k)}{\partial t}+\frac{\partial\left(\rho v_j k\right)}{\partial x_j}=\frac{\partial}{\partial t}\left[\frac{\mu_e \partial k}{\varepsilon_k \partial x_j}\right]+P-\rho\varepsilon \tag{12}$$

$$\frac{\partial(\rho\varepsilon)}{\partial t}+\frac{\partial\left(\rho v_j \varepsilon\right)}{\partial x_j}=\frac{\partial}{\partial x_j}\left[\frac{\mu_e \partial \varepsilon}{\varepsilon_e \partial x_j}\right]+\frac{\varepsilon}{k}\left(c_{1\varepsilon}P-\rho c_{2\varepsilon}\varepsilon\right)-c_3\frac{\varepsilon}{k}P \tag{13}$$

where v is the vector of the velocity (m/s), P is the flow pressure (Pa), x_j is the component of j direction, k is the turbulence energy, ε is the dissipation rate, ρ is the density (kg/m^3), and μ_e is the viscosity. $C_{1\varepsilon}$, $C_{2\varepsilon}$, and $C_{3\varepsilon}$ are the constants. $C_{1\varepsilon}=1.44$, $C_{2\varepsilon}=1.9$, and $C_{3\varepsilon}=0.09$.

Table 1 Geometry parameters and boundary conditions

Parameters	Values tested	Typical value
Cutting pressure (MPa)	380	250–400
Abrasive flow rate (g/s)	7	3.8–11.2
Abrasive solid	Garnet (#80)	Garnet (#80–#150)
Orifice diameter (mm)	0.38	0.025–0.43
Mixing chamber diameter (mm)	5	4–7
Mixing chamber length (mm)	10	10–20
Particle inlet diameter (mm)	3	3–5
Particle inlet position (mm)	Low, mid, high	N/A
Particle inlet angular (°)	0, 30, 45	0
Converging part angular (°)	60, 70, 80	60
Focusing tube diameter (mm)	1.14	0.5–1.3
Focusing tube length (mm)	76	50–112

N/A not available

For the continuous phase, the pressure inlet boundary condition was applied to the primary flow (water). A water pressure inlet P_w is a constant number (380 MPa) which is a typical operating pressure for ultrahigh-pressure AWJ applications provided by the pump. In the current simulation, the air and abrasives are naturally sucked into the mixing chamber by the Venturi effect. Thus, the abrasive pressure (equals to air pressure) P_a was set to 0.101325 MPa (atmospheric pressure) at the initial inlet. The atmospheric pressure is also applied at the pressure outlet of the focusing tube exit. The no-slip velocity condition is imposed on the wall boundaries. For the particle phase, uniform velocities are applied at the abrasive particle inlet with a specified particle mass flow of 7 g/s with the inlet direction normal to the boundary.

4 Simulation procedure and model validation

4.1 Simulation procedure

The second-order upwind scheme was used for the advection terms in the equations governing mass conservation, momentum, and turbulence closure in this study because it can obtain more reliable results consuming little more time compared to the first-order. The PRESTO! algorithm is applied to approximate the pressure value. There is also need to set solution monitor to prevent unacceptable results or ensure the results converged. When the water-air flow field solution is obtained, abrasive particles are added to the multiphase flow through the abrasive inlet tube. Then, particle velocities and particle trajectories are calculated and statistically analyzed. Five hundred iterations with erosion/acceleration model were tracked and investigated in the cases. The outlet boundary for dispersed phase is set as "escape," which means that the trajectory tracking calculation is stopped once the particle reaches

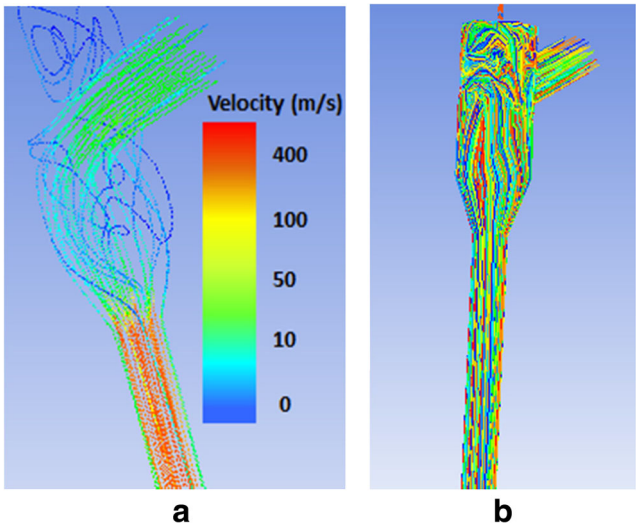

Fig. 3 Detailed particle velocity (**a**) and movement (**b**)

the boundary. Moreover, the particle interaction is modeled using the mentioned Bond's comminution model [12]. After the residuals of solutions converged, the results were obtained by using the post processor CFD-Post, seen in Fig. 3.

4.2 Validation of the established physical model

There are already lots of experiments done to monitor the air flow rate at the abrasive feeding pipe and air-water velocity ratio in the focusing tube [17, 18, 25, 26]. As the established physical model, as well as the corrective boundary conditions, needs confirmation, comparison investigation was carried out between simulation model and the aforementioned practical experiments under the same settings.

4.2.1 Comparison about air volume flow

Recently, M. Putz et al. [18] have performed the observation of the air volume flow by using a single-pipe flow measuring system that had been attached inside the abrasive supply hose. Ideally, it is possible to detect blockages of the abrasive particle supply as well. The experimental and the simulation results indicate there is a good agreement shown in Fig. 4.

4.2.2 Comparison of air-water jet velocity ratio

A.H. Osman [17] used static pressure tap at the various locations along the flow direction. A clear mixing head was manufactured, to measure the visible experiments of the water jet, observed by using a Canon HC-1000 camera. The value of pump pressure is 50, 100. 140, 180, and 220 MPa, respectively. The ratio of the air flow to the water jet velocities (V_a/V_j) at the middle of the tube was evaluated for different diameter ratios (R_{mn}) and a clear mixing head was manufactured; the simulation results are accurate with a total error of 7.9%

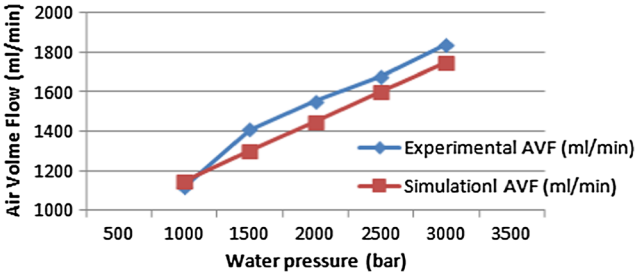

Fig. 4 Air flow measurement under different pump pressure

(shown in Fig. 5). This error may be caused by some water vapor appearing in the tube.

4.2.3 Comparison about particle speed

Recently, Balz et al. [19, 20] have performed ultra-fast X-ray velocimetry experiments to measure velocities and spatial positions of abrasive particles within the three-phase (air-fluid-solid) flow. A third-generation synchrotron light source (SLS) provided sufficient photon flux to take double images of the AWJ with an inter-frame time interval of 5 μs. Table 2 also proves that the simulation average abrasive velocity has a relatively low error with the data from SLS experiments.

From the quantitative information showed above, we validate the established model from three different aspects where every parameter has a significant impact on AWJ performance. Meanwhile, it is also the first time to use simulation method to detect air volume flow rate and air velocity during mixing progress. Furthermore, comparisons mentioned above have a good consistency corresponding to the experimental results which makes future work more accurate and reliable.

5 Results and discussion

5.1 Flow field inside of AWJ cutting head

When the high-pressure water gets out of the orifice, the ultrahigh-speed water jet is formed with a typical jet velocities up to 900 m/s at 380 MPa. The flow into the mixing chamber creates a vacuum, transporting abrasives from feeding pipe into the chamber via a suction effect (Venturi effect). The abrasives are accelerated and axially oriented (focused) in the mixing tube so that a hard and tough material such as tungsten carbide is used as a mixing tube to resist erosion. Otherwise, the jet diameter will become larger during processing, causing poorer workpiece roughness. The water-solid multiphase flow in the AWJ cutting head can be indicated in Fig. 3. The abrasive flow is assumed to be uniform in the feed pipe following the direction which is normal to the boundary of air feed pipe because the particles are entrained by air flow. When the abrasive particles enter into mixing chamber, there will be a swirl flow around the water jet due to the large

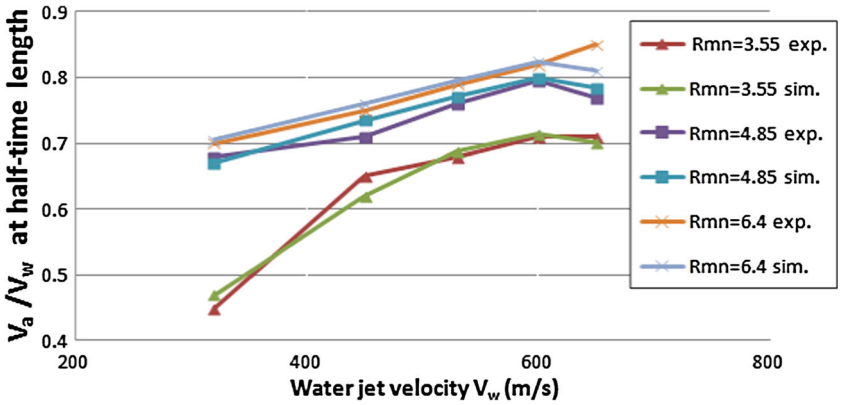

Fig. 5 Air-water jet velocity ratio at the middle of the tube versus the water jet velocity for different diameter ratios R_{mn}

velocity gradient between water and solid. At first stage of interaction, it is hard for garnets to enter into the jet core to get full acceleration because of the speed jag. This kind of phenomenon may drag the particles, conducting circumferential movements and some rebound collision both between particles and walls [27] which will result in more energy dissipation, weakening the AWJ machining performance.

5.2 Effect of particle inlet angle

5.2.1 Particle inlet angle impacting on AWJ velocity

Figure 6a shows the water and particle mean velocities along the length of AWJ cutting head under the influence of different abrasive particle inlet angles from 0° to 60°. Right now, the most widely applied design is 0°, seen in Fig. 1. In this study, different inlet angles of particle entry were analyzed. From the top line of Fig. 6a, it indicates that the water velocity keeps decreasing within the cutting head as there are wall friction and energy exchange with other phases. As a typical cutting head design, 76.2 mm is one of the typical size manufacturers will choose because if it is too short, the particle will not get fully accelerated by water momentum. Figure 6a shows the velocity of abrasive flow can nearly reach stable at a distance of 10 mm before exiting the focusing tube, which proves our numerical model is acceptable. However, since the water jet disintegrates by the acceleration process of air (leads to wall shear), along with a shock occurring at the exit region of the focusing tube (recompression phenomenon) [17], the velocity ratio V_p/V_w downstream cannot reach 1, which can be observed clearly from Fig. 6a. Due to the relatively higher speed of water jet and momentum exchange, it is hard for particles to enter the center zone of the jet. Meanwhile, it is interesting that when we choose inlet angle 60°, the velocity is nearly the best of all other angles. One reason is that the suction effect makes the particle obtain larger axial velocity and smaller radial velocity when they enter mixing chamber, which means the particles are easily mixed and carried by high-speed jet as shown in Fig. 3b. From the simulation results, the outlet means velocity under 60° angle is 7.62% higher than traditional design. With bigger inlet angle, the particle velocity seems to increase more quickly, and the final particle outlet velocity also gets higher. One possible explanation for this may be the more efficient drag force on the particle movement.

Table 2 Test results conducted by SLS experiments and Fluent computation

Exp.	Pressure (MPa)	Abrasive flow (g/s)	SLS avg. abrasive vel. (m/s)	Simulation avg. abrasive vel. (m/s)	Relative error (%)
1	90.98	3.52	251.00 ± 50.2	275.89	9.80
2	142.79	3.83	305.60 ± 52.3	332.72	8.87
3	195.20	4.45	353.60 ± 59.3	380.78	7.64
4	296.70	5.5	450.40 ± 63.9	486.22	7.91
5	355.34	6.17	482.00 ± 82.1	531.19	10.20

5.2.2 Particle inlet angle impacting on nozzle wear

At the same time, to investigate the nozzle wear (including mix chamber and the focus tube) and improve the lifetime of cutting head, different inlet angles are taken into consideration, seen in Fig. 6b. In a typical wear test, the exit diameter and weight of the nozzle are recorded before it is installed in the cutting head. The nozzle bore profile can be found out by sectioning the nozzle longitudinally and measuring the profile using white light interferometry which is a non-contact optical method for surface measurement on 3D structures. For the simulation part, we can get discrete phase model (DPM) erosion rate by checking DPM variables contour in the FLUENT results. By applying these methods, we can obtain different wears at different positions of the focusing tube. It also indicates larger particle inlet angle has a better anti-wear performance over other choices. With bigger inlet angle, the nozzle wear region seems to decrease more quickly, and the initial intensive erosion region also occupies the

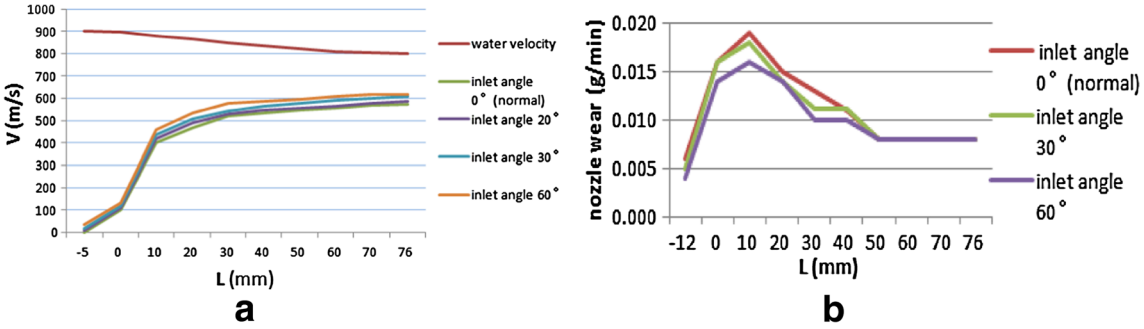

Fig. 6 Effect of inlet angle on **a** AWJ velocity and **b** nozzle wear

relatively small area. One reasonable explanation for it is more coefficient for particle movement during mixing progress, making more energy used for accelerating solids. On the other hand, increasing the inlet angle makes particles get more axial acceleration which can ensure solids enter focusing tube more easily, reducing particle wall collision and rebound times. While at the downstream part of a focus tube, the wear rates of three conditions are the same since the particles are accelerated at the downstream of cutting head, although the particle radial velocity can be much different from that of the first stage. From Fig. 6a, we can know the final axial speeds are close to each other to some extent, and that can be one reason why the wear rate is the same in the downstream region.

5.3 Effect of particle inlet position

5.3.1 Particle inlet position impacting on AWJ velocity

Shown in Fig. 7a, the particle acceleration rate increases rapidly from − 5 to 20 mm. This is because the velocity of solid is quite low compared with water jet, so the acceleration rate is high from − 5 to 0 mm. However, when the particles enter focusing tube in the conical structure, the water particle mixed in a small space where exits intense energy exchange. After this, the rising rate becomes stable, boosting solid speed gradually. In Fig. 7a, there is no water velocity for the condition of inlet position low and mid at the – 5-mm distance from the entry of focusing tube as the particle flow just arrives mixing chamber, and there is no impact force on them.

5.3.2 Particle inlet position impacting on nozzle wear

From Fig. 7b, we can see inlet at a higher place indicates less nozzle wear under the same processing time too. For solid feed pipe at a low position, some radial jet backflow will carry particles with disorder movement in the mixing chamber which leads to low axial velocity and produces a wall-particle collision. This is why there are largest wear areas when putting inlet hole at bottom place compared with others seen in Fig. 7b. At the same time, some backflow water may also wet abrasive inlet hole and degrade suction effect. This phenomenon is what we need to prevent. Otherwise, it will reduce AWJ machining efficiency. In comparison with three final velocity rates V_p/V_w, 76% obtained from a high position, 73.5% earned from the normal position, and 72% achieved from low position, respectively. Meanwhile, higher inlet hole is recommended under the same machining cost. Therefore, it is a good choice for a designer to put particle inlet into a top position, resulting in faster outlet velocity and less nozzle wear volume.

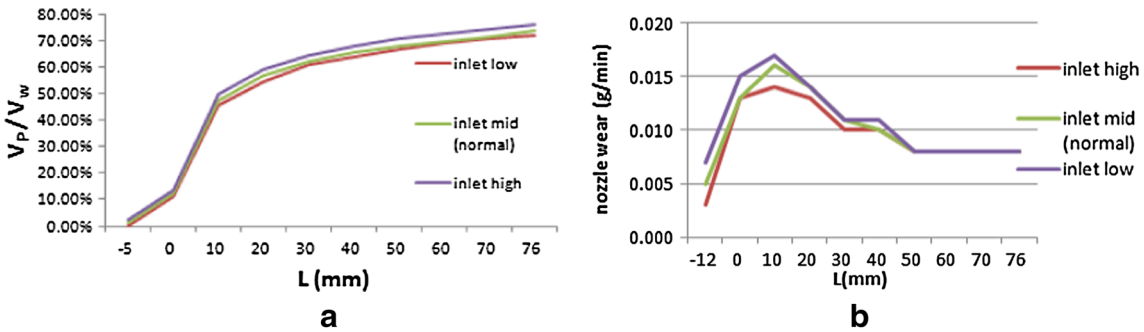

Fig. 7 Effect of inlet angle on **a** particle acceleration rate and **b** nozzle wear

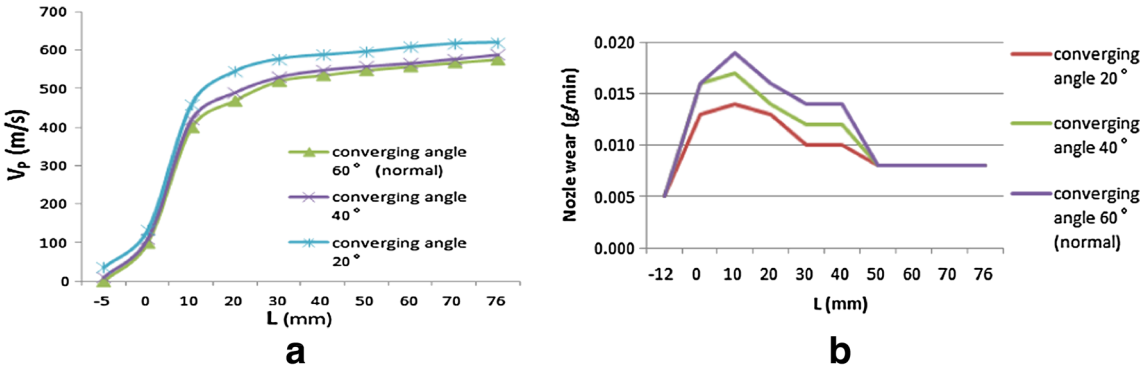

Fig. 8 Effect of converging angle on **a** particle mean velocity and **b** nozzle wear

5.4 Effect of focusing tube converging angle

5.4.1 Focusing tube converging angle impacting on AWJ velocity

Figure 8 shows the particle velocity evolutions with different converging angles at the entry of focusing tube. The smallest taper angle tends to accelerate the solid more effectively under the same mixing length. Compared with other converge angles, the final exit velocity also shows higher performance for closely 5% over other designs. At the initial mixing stage, the particle speed at converging angle 20° is a little bit higher than other two structures because there is much fewer backflow generated from conical entry.

5.4.2 Focusing tube converging angle impacting on nozzle wear

Observed from Fig. 8b, it also shows that there is less mass removal rate for converge angle 20°. This phenomenon is more recognized than other impact factors, stressing the importance of converge angle. This can be attributed to these reasons as follows: When the converging angle becomes smaller, it will also lengthen the focus distance. Then, it makes sure particles earn more axial speed and less radial energy. At the same time, there is fewer backflow jet separated from water jet edge, promising more kinetic energy used to accelerate solids.

6 Conclusion

In this study, CFD simulations based on Euler-Lagrange methodology have been carried out to investigate the internal jet flow and the particle mixing progress in the AWJ cutting head. The physical model and the boundary conditions are verified by previous experiments. Three parameters that influence solid acceleration and nozzle wear were studied in detail. The effects of these factors on AWJ exit velocity and nozzle weight loss are summarized as follows:

1. Particle inlet angle degrees influence AWJ exit velocity. With the larger inlet angle (60°), the final solid speed is 7.62% higher than normal design.
2. The effect of increasing the inlet angle results in reduced wall wear near the area where solid velocity change rapidly.
3. The position of particle inlet has a negative effect on water speed gradient. However, the effect of inlet hole position on solid acceleration is biggest when the pipe hole was at high level.
4. The particle inlet position has a similar impact trend on nozzle wear compared with particle inlet angle. At the downstream of the jet, the wear rate is stable and shows an insignificant difference.
5. The effect of converging angle of focusing tube on two measured results is significant. The final velocity is 5% higher and the nozzle weight loss is 16.23% lower, respectively, in comparison with the typical nozzle structure.

Acknowledgements The authors thank Dr. Sawhney for his assistance in giving advice on conducting the simulation experiments.

Funding This work is financially supported by the National Natural Foundation Program (51575237) and 2016 International Cooperation & Training Program for Creative Talents (File No. 201600090095).

References

1. Zhu HT, Huang CZ, Wang J, Li QL, Che CL (2009) Experimental study on abrasive waterjet polishing for hard–brittle materials. Int J Mach Tools Manuf 49(7-8):569–578. https://doi.org/10.1016/j.ijmachtools.2009.02.005
2. Prisco U, D'Onofrio MC (2008) Three-dimensional CFD simulation of two-phase flow inside the abrasive water jet cutting head. Int J Comput Methods Eng Sci Mech 9(5):300–319. https://doi.org/10.1080/15502280802225598
3. Wang J (2009) Particle velocity models for ultra-high pressure abrasive waterjets. J Mater Process Technol 209(9):4573–4577. https://doi.org/10.1016/j.jmatprotec.2008.10.021
4. Hoogstrate AM, Susuzlu T, Karpuschewski B (2006) High performance cutting with abrasive waterjets beyond 400 MPa. CIRP Ann

Manuf Technol 55(1):339–342. https://doi.org/10.1016/S0007-8506(07)60430-2
5. Axinte DA, Karpuschewski B, Kong MC, Beaucamp AT, Anwar S, Miller D, Petzel M (2014) High energy fluid jet machining (HEFJet-Mach): from scientific and technological advances to niche industrial applications. CIRP Ann Manuf Technol 63(1): 751–771. https://doi.org/10.1016/S0007-8506(07)60430-2
6. Barletta M, Tagliaferri V (2006) Development of an abrasive jet machining system assisted by two fluidized beds for internal polishing of circular tubes. Int J Mach Tools Manuf 46(3-4):271–283. https://doi.org/10.1016/j.ijmachtools.2005.05.014
7. Momber AW, Kovacevic R (2012) Principles of abrasive water jet machining. Springer Science & Business Media, Berlin
8. Liu D, Huang C, Wang J, Zhu H, Yao P, Liu Z (2014) Modeling and optimization of operating parameters for abrasive waterjet turning alumina ceramics using response surface methodology combined with Box–Behnken design. Ceram Int 40(6):7899–7908. https://doi.org/10.1016/j.ceramint.2013.12.137
9. Li Z, Geskin E, Tismenetskiy L (1994) Improvement of water-particles mixing in the course of abrasive waterjet formation. ASME-PUBLICATIONS-PED 68:405–405
10. Osman, A., Buisine, D., Thery, B. and Houssaye, G (1996) Measure of air flow rate according to the mixing chamber designs. In BHR Group Conference Series Publication 21:223-236. Mechanical Engineering Publications Limited
11. Narayanan C, Balz R, Weiss DA, Heiniger KC (2013) Modelling of abrasive particle energy in water jet machining. J Mater Process Technol 213(12):2201–2210. https://doi.org/10.1016/j.jmatprotec.2013.06.020
12. Hou R, Huang C, Zhu H (2013) Numerical simulation of multi-phase flow field in abrasive waterjet machining. Int J Abras Technol 6(1):40–57. https://doi.org/10.1504/IJAT.2013.053166
13. Teymoori F, LohMousavi M, Etesam A (2016) Numerical analysis of fluid structure interaction in water jet incremental sheet forming process using coupled Eulerian–Lagrangian approach. Int J Interac Des Manuf 10(2):203–210. https://doi.org/10.1007/s12008-013-0197-9
14. Hou R, Huang C, Zhu H (2014) Numerical simulation ultrahigh waterjet (WJ) flow field with the high-frequency velocity vibration at the nozzle inlet. Int J Adv Manuf Technol 71(5-8):1087–1092. https://doi.org/10.1007/s00170-013-5493-9
15. Li H, Lee A, Fan J, Yeoh GH, Wang J (2014) On DEM–CFD study of the dynamic characteristics of high speed micro-abrasive air jet. Powder Technol 267:161–179. https://doi.org/10.1016/j.powtec.2014.07.018
16. Al-Bukhaiti MA, Abouel-Kasem A, Emara KM, Ahmed SM (2016) Particle shape and size effects on slurry erosion of AISI 5117 steels. J Tribol 138(2):024503. https://doi.org/10.1115/1.4031987
17. Osman AH, Mabrouki T, Thery B, Buisine D (2004) Experimental analysis of high-speed air–water jet flow in an abrasive water jet mixing tube. Flow Meas Instrum 15(1):37–48. https://doi.org/10.1016/j.flowmeasinst.2003.08.001
18. Putz M, Dittrich M, Dix M (2016) Process monitoring of abrasive waterjet formation. Procedia CIRP 46:43–46. https://doi.org/10.1016/j.procir.2016.03.189
19. Balz R, Heiniger KC (2011) Determination of spatial velocity distributions of abrasive particles in abrasive water jets using laser-induced fluorescence under real conditions. In Proceedings of 16th WJTA-IMCA Conference and Expo
20. Balz R, Mokso R, Narayanan C, Weiss DA, Heiniger KC (2013) Ultra-fast X-ray particle velocimetry measurements within an abrasive water jet. Exp Fluids 54(3):1476. https://doi.org/10.1007/s00348-013-1476-8
21. Wang R, Wang M (2010) A two-fluid model of abrasive waterjet. J Mater Process Technol 210(1):190–196. https://doi.org/10.1016/j.jmatprotec.2009.06.007
22. Miller D (2004) Fluid dynamics of abrasive waterjet cutting heads. In Proceedings of the 17th International Conference on Water Jetting, Cranfield, Mainz, Germany, BHR Group Limited, pp 107–121
23. Ansys AF. 14.0 (2011) Theory guide. ANSYS Inc, Canonsburg, pp 218–221
24. Thanomputra S, Kiatiwat T (2016) Simulation study of cutting sugarcane using fine sand abrasive waterjet. Agric Nat Resour 50(2):146–153. https://doi.org/10.1016/j.anres.2015.10.001
25. Hashish M (2003) Inside AWJ nozzles. In Proc. of the WJTA American Waterjet Conference, pp 243-260
26. Sou A, Hosokawa S, Tomiyama A (2007) Effects of cavitation in a nozzle on liquid jet atomization. Int J Heat Mass Transf 50(17-18): 3575–3582. https://doi.org/10.1016/j.ijheatmasstransfer.2006.12.033
27. Nanduri M, Taggart DG, Kim TJ (2000) A study of nozzle wear in abrasive entrained water jetting environment. J Tribol 122(2):465–471. https://doi.org/10.1115/1.555383